AFRL-RX-WP-TP-2009-4119

MICROSTRUCTURAL CHANGES AND ESTIMATED STRENGTHENING CONTRIBUTIONS IN A GAMMA ALLOY Ti-45Al-5Nb PACK-ROLLED SHEET (PREPRINT)

Y-K. Kim, A. Rosenberger and D.M. Dimiduk

UES, Inc.

APRIL 2009

AIR FORCE RESEARCH LABORATORY
MATERIALS AND MANUFACTURING DIRECTORATE
WRIGHT-PATTERSON AIR FORCE BASE, OH 45433-7750
AIR FORCE MATERIEL COMMAND
UNITED STATES AIR FORCE

REPORT DOCUMENTATION PAGE

Form Approved
OMB No. 0704-0188

1. REPORT DATE *(DD-MM-YY)*	2. REPORT TYPE	3. DATES COVERED *(From - To)*
April 2009	Journal Article Preprint	01 April 2009- 01 April 2009

4. TITLE AND SUBTITLE
MICROSTRUCTURAL CHANGES AND ESTIMATED STRENGTHENING CONTRIBUTIONS INA GAMMA ALLOY Ti-45Al-5Nb PACK-ROLLED SHEET (PREPRINT)

5a. CONTRACT NUMBER
FA8650-04-D-5235

5b. GRANT NUMBER

5c. PROGRAM ELEMENT NUMBER
62102F

6. AUTHOR(S)
Y-W. Kim (UES, Inc.)
A. Rosenberger and D.M. Dimiduk (AFRL/RXLM)

5d. PROJECT NUMBER
2511

5e. TASK NUMBER
00

5f. WORK UNIT NUMBER
25110002

7. PERFORMING ORGANIZATION NAME(S) AND ADDRESS(ES)
UES, Inc.
4401 Dayton-Xenia Road
Dayton, OH 45433-7817

8. PERFORMING ORGANIZATION REPORT NUMBER
AFRL-RX-WP-TP-2009-4119

9. SPONSORING/MONITORING AGENCY NAME(S) AND ADDRESS(ES)
Air Force Research Laboratory
Materials and Manufacturing Directorate
Wright-Patterson Air Force Base, OH 45433-7750
Air Force Materiel Command
United States Air Force

10. SPONSORING/MONITORING AGENCY ACRONYM(S)
AFRL/RXLMD

11. SPONSORING/MONITORING AGENCY REPORT NUMBER(S)
AFRL-RX-WP-TP-2009-4119

12. DISTRIBUTION/AVAILABILITY STATEMENT
Approved for public release; distribution unlimited.

13. SUPPLEMENTARY NOTES
To be submitted to Intermetallics (Elsevier Ltd Publication)
PAO Case Number and clearance date: 88ABW-2009-1027, 16 March 2009.
The U.S. Government is joint author of this work and has the right to use, modify, reproduce, release, perform, display, or disclose the work.

14. ABSTRACT
Thin sheets made of a gamma-titanium aluminide alloy, Ti-45Al-5Nb, produced by a patented pack-rolling process, were evaluated for microstructure variation and evolution taking place during aging and annealing treatments. The as-received sheet material was characterized by remarkably high yield strength, 810MPa, and a complex bimodal microstructure. The microstructure consisted of a matrix of twinned gamma-phase grains and fine-lath lamellar-grain microconstituent, together with a dispersed ultra-fine-grained gamma + alpha-2 mixture microconstituent. High-temperature isothermal aging treatments changed the microstructure to a stable mixture of gamma-phase grains (matrix) and coarse alpha-2 phase particles, having size distributions and volume fractions that were specific to the aging temperature. A concurrent strength loss reflects this trend and results in a stable strength level of 550 MPa upon aging at 1000°C for 144h. Using composition estimates from the phase-boundary shifts that occur from the Nb addition to a Ti-45Al base alloy and, the rule of mixtures, an analysis was made to show that the gamma- phase matrix has an intrinsic strength of 178MPa. This is a significant intrinsic strength level, well over that of ~70MPa for the Ti-45Al binary alloy. This is rationalized as the solid-solution strengthening effect from shifts of the Ti and Nb levels in the gamma phase and, by an added effect due to increased oxygen solubility in the gamma phase. The overall strength of Ti-45Al-5Nb, however, is roughly the same as that of Ti-45Al, and this is explained by a drastic reduction in the volume fraction of alpha-2 phase in Ti-45Al-5Nb alloy, which is a result of the Nb-induced phase-boundary shifts.

15. SUBJECT TERMS
gamma-titanium aluminide, Ti-45Al-5Nb, pack-rolling process

16. SECURITY CLASSIFICATION OF:			17. LIMITATION OF ABSTRACT:	18. NUMBER OF PAGES	19a. NAME OF RESPONSIBLE PERSON (Monitor)
a. REPORT	b. ABSTRACT	c. THIS PAGE			Christopher Woodward
Unclassified	Unclassified	Unclassified	SAR	34	19b. TELEPHONE NUMBER *(Include Area Code)* N/A

(022609-YWK) To be Submited to Intermetallics

Microstructural Changes and Estimated Strengthening Contributions in a Gamma Alloy Ti-45Al-5Nb Pack-Rolled Sheet

Y-W. Kim*, A. Rosenberger and D. M. Dimiduk Air Force Research Laboratory, AFRL/MLLM, Wright-Patterson AFB, OH 45433, USA (*UES, Dayton, OH 45432, USA)

Abstract

Thin sheets made of a gamma-titanium aluminide alloy, Ti-45Al-5Nb, produced by a patented pack-rolling process, were evaluated for microstructure variation and evolution taking place during aging and annealing treatments. The as-received sheet material was characterized by remarkably high yield strength, 810MPa, and a complex bimodal microstructure. The microstructure consisted of a matrix of twinned gamma-phase grains and fine-lath lamellar-grain microconstituent, together with a dispersed ultra-fine-grained gamma + alpha-2 mixture microconstituent. High-temperature isothermal aging treatments changed the microstructure to a stable mixture of gamma-phase grains (matrix) and coarse alpha-2 phase particles, having size distributions and volume fractions that were specific to the aging temperature. A concurrent strength loss reflects this trend and results in a stable strength level of 550 MPa upon aging at 1000°C for 144h. Using composition estimates from the phase-boundary shifts that occur from the Nb addition to a Ti-45Al base alloy and, the rule of mixtures, an analysis was made to show that the gamma- phase matrix has an intrinsic strength of 178MPa. This is a significant intrinsic strength level, well over that of ~70MPa for the Ti-45Al binary alloy. This is rationalized as the solid-solution strengthening effect from shifts of the Ti and Nb levels in the gamma phase and, by an added effect due to increased oxygen solubility in the gamma phase. The overall strength of Ti-45Al-5Nb, however, is roughly the same as that of Ti-45Al, and this is explained by a drastic reduction in the volume fraction of alpha-2 phase in Ti-45Al-5Nb alloy, which is a result of the Nb-induced phase-boundary shifts.

1. Introduction

Gamma TiAl alloy sheets are generally produced by a pack-rolling process that was first explored during the early 90's [1] and further developed to a production process over fifteen years through the early 2000's [2, 3]. At the end of the development period, Plansee was able to produce sheets (0.5-1mm thick) as large as (50cm x 250cm) as well as foils (150-75μm) having sizes up to (2cmx150cm). Alloys that Plansee has used for rolling include experimental alloys [2], an engineering alloy called "Gamma Met," Ti-46.5Al-4(Cr,Nb,Ta,B), "XD alloys" (Ti-45Al-2Nb-2Mn-0.8vol%TiB_2), "K5 alloys" (Ti-(46-46.5)Al-3Nb-2Cr-0.2B-0.2C-015Si) and, high Nb-containing engineering alloys including Ti-45Al-(5-10)Nb-xB.

Sheets are typically given an annealing treatment for stress relief and stabilization, and the resulting fine-grained microstructures yield greater strength levels than conventionally-processed, fine-grained material. In sheets, a major strengthening effect is expected to be extrinsic; that is, rolling-induced finely deformed structures. These, however, have not been quantified nor understood because of difficulties in conducting experiments. The deformed structures are often too complex for quantitative analysis. The recovery, recrystallization and microstructure evaluation processes leading to the deformation-free state must be followed by careful microstructure observations and quantification, together with corresponding strength-variation measurements. In the case of high-Nb containing alloys, another major contribution to strength is expected from the decreases in Al content [4, 5] and increases in Nb content [6]. Most gamma TiAl alloys are essentially two-phase (γ+α_2) mixtures and occasionally contain small amounts of beta-phase particles. In general, lowering the Al content increases the alpha-2/gamma volume ratio and thereby the alloys become harder because of the increased volume fractions of the hard alpha-2 phase. Whether or not Nb additions affect the strength levels has been neither isolated nor quantified, although in the single-phase Ti-50Al-(0-10)Nb system the room-temperature (RT) hardness was reported to gradually increase with Nb content [7, 8].

Several attempts have been made to explain the measured strength increases in the two-phase alloy system Ti-(45-49)Al-(5-10)Nb. The two most prevailing but contradicting explanations are solid-solution hardening of the gamma phase by Nb [9] and structural refinement, especially during deformation via abundant twinning [4, 10]. Recently, however, we have observed that both interpretations neglect the basic phase relationships such as changes in composition and volume fraction of the constituent phases. Changes to the positions of phase boundaries will also lead to a variation in interstitial contents within the phases [5]. These complex occurrences are expected to not only alter the strength level of each phase, but also their relative contribution to the system's strength, thus making isolation of each effect on strengthening complex.

This paper reports our recent effort to understand strengthening mechanisms in alloy Ti-45Al-5Nb-0.2B sheet material, called "Gamma Met PX," produced by Plansee.

Microstructural evolution, stability and the resulting strength variation were investigated in detail as a function of temperature as part of the study and, the results are used to help interpret the complex mechanisms.

2. Experimental Procedure

Pieces of 1mm thick Gamma Met PX pack-rolled and ground sheet were received in the usual post-roll annealed condition (1000°C/2h). Pack-rolling had been conducted on a preform made of a hot-worked ingot plate at temperatures within the upper region of the $\alpha+\gamma$ phase field. Coupon specimens were sectioned from the sheet and given various annealing treatments at temperatures above 1100°C and, aging treatments at temperatures below 1100°C according to the conditions discussed later. Heat-treatment temperatures were selected using preliminary heat-treatment experiments and differential thermal analysis (DTA) results. Heat treatments were conducted either in a vacuum furnace or in argon-filled quartz tubing. In the latter case, the tubing was broken outside the furnace and then samples were cooled in air. Samples were mounted in conductive mounts and polished to 0.06µm finish through carefully-controlled grinding and mechanical-polishing processes. All samples were mounted to have the short transverse (ST) plane up, while the as-received samples were sectioned and mounted to reveal all planes, including the long transverse (LT) and longitudinal or rolling plane (L). The designation of the planes is defined in the results section. For the as-received condition, TEM foils for the L plane were also prepared for detailed microstructure observations using conventional twin-jet and ion-mill processes. In both as-received and heat-treated conditions, samples were characterized for microstructure distribution, evolution and stability and compositional spatial variation. These were achieved using light microscopy, electron microscopy (BEI, EDS, X-ray mapping) and electron back-scattered diffraction (EBSD). Vickers micro-hardness measurements were made before and after heat treatments and the data was converted to values of estimated tensile yield strength. The conversion process is explained in the result section. The equilibration process following the treatments was tracked by correlating the strength and microstructure variations as a function of heat-treatment condition.

3. Results

3.1 As Received Sheet Microstructures and Compositions

The as received sheet samples were examined using the back-scattered electron imaging (BSEI) conditions. The overall microstructures, as taken from the rolling plane (L) as well as the short transverse plane (ST) at low magnifications, are shown in Figure 1. Another plane, the long transverse (LT), is defined as the plane perpendicular to the rolling direction (RD) and transverse to the plane of the sheet. The rolling plane contains a fine but fairly non-uniform distribution of somewhat elongated grains that

form a mixture of coarse-grained and fine-grained regions. Coarse grains are imaged either as gray or bright, indicating there are two different groups distinguishable (perhaps) by their composition. Although taken at an even lower magnification, the microstructures taken from the ST plane (thickness plane parallel to the RD) show a fine and relatively uniform grain-size distribution. The thickness of the sheet is measured to be 1mm (1000μm). In Figure 2a and 2b, BSEI images taken from both ST (Figures 2a and 2c) and LT (Figure 2b) planes at a higher magnification are shown, with each having a uniform distribution of grains but also an apparent morphological directionality. OIM image analysis for the ST plane in Figure 2c clearly indicates that the as-received microstructure is bimodal in grain-size distribution having relatively coarse grains, often containing twin-like features, and much finer grains that appear to be present as groups (Figure 2c). The grain sizes determined by the EBSD imaging analysis on the Figure 2C plane range from submicron to nearly 20μm, as shown in Figure 2d. There appears to be a cutoff between the two groups of grains at around 3μm. Taking all sizes into consideration, the analysis suggests that the average grain size in the viewing area of Figure 2c is ~6.0μm.

In order to understand the details of the bimodal structures, TEM foils were prepared from the L plane. It was found that the TEM foils were extremely helpful for BSEI examination, as well as for EBSD analysis. An EBSD microstructure taken from a TEM foil using a 0.2μm beam step (Figure 3) clearly reveals the bimodal grain size in detail. There are two groups of coarse grains in terms of their appearance; one is featureless and the other contains twins. Fine (~3μm or smaller) grains are present as agglomerates, often decorating coarse gamma-phase grains, Figure 3. As shown later, the fine grains are essentially gamma-phase grains that are either pinned by or, mixed with, residual alpha-2-phase particles.

Detailed microstructural features in the as-received sheet were observed on the rolling plane (L) by BSE imaging of TEM foils, as shown in Figure 4. Several important features are apparent. The coarse grains that imaged having bright (“L1”) to light-gray contrast (“L2”) consist of ultra-fine lath structures wherein the formation of gamma-phase laths is only in the beginning or partially complete, as respectively shown by the lath grains at “L1” (Figure 4a) and “L2” (Figure 4b). Coarse grains imaged having a gray to dark appearance in Figure 4, consist of either well-advanced lath structures (as are the cases for grains “G’s”) or contain deformation twins (as are the cases for grains “B’s”). The fine-grained regions in Figure 3 are actually agglomerates of gamma-phase grains (indicated by “F” in Figure 4) mixed with a substantial volume fraction of fine alpha-2-phase particles which decorate gamma-phase grain boundaries. Judging from the morphologies, partial recrystallization may have happened in region “F” of Figure 4b, resulting in apparent growth of fine gamma-phase grains into the lath grain L_B.

The composition distribution of the elements Ti, Al and Nb, on ST and L planes, was analyzed by electron probe microanalysis (EPMA) and the results are plotted as a function of position along line scans in Figure 5. A 20μm diameter electron beam was

used to analyze 150 areas on each plane along a linear length of 3mm in the rolling direction, each being 20μm apart. From the data, the average composition (at%) on each plane was calculated and both compositions were found to be essentially the same as listed below.

Ti-44.66Al-5.43Nb (at%) (on ST plane)
Ti-44.63Al-5.43Nb (at%) (on L plane)

On both planes, the Nb concentration is constant and uniform along the length analyzed. On the other hand, both Al and Ti concentrations vary noticeably from location-to-location, with greater variation occurring on the rolling plane (L), which is consistent with the BESI observations shown in Figure 1. Figures 5c and 5d accentuate the variations of Al and Ti contents using a higher-resolution scale to show their ranges as follows:

(48.6-51.0)Ti-(43.3-46.0)Al (at%) (ST plane)
(48.2-51.3)Ti-(43.1-46.5)Al (at%) (L plane)

The alpha transus temperature ($T\alpha$) of the Gamma Met PX alloy was measured on the as-received sheet material using the DTA method. From the endothermic peak of the second-cycle heating curve, obtained under a heating rate of 30°C/min, the value was determined to be 1318°C.

3.2 Heat Treatments and Hardness Variation

Table 1 lists the conditions for annealing and aging treatments conducted on the as-received sheet material, designated as PX0. Group PXA samples were annealed at temperatures in the range from 1200° to 1350°C, which covers most parts of the ($\alpha+\gamma$)-phase field (1200°C-1318°C), and a lower part (1318-1350°C) of the α-phase field. The purpose of annealing treatments was to see how the new microstructures evolve at the expense of the existing microstructures. Group PXB, PXC and PXD samples were given aging treatments at temperatures between 700°C and 1000°C. The aging treatments were aimed to recover and recrystallize the deformed microstructures and, to equilibrate the composition as well as the volume fractions of constituent phases. In this way, the intrinsic strengthening could be isolated from the contributions from extrinsic aspects such as processing (rolling deformation) and non-equilibrium distribution of phase and/or composition. Following each treatment, fifteen Vickers-hardness measurements were made on each of the samples and the values of hardness were averaged. The average hardness value (Hv) for each condition was plotted against its corresponding heat-treatment condition as shown in Figure 6. The right-hand Y-axis in Figure 6 shows the corresponding yield stress (YS) that was estimated using the hardness-yield stress relationship [11-13] that was empirically established as discussed later.

From Figure 6, it is clear that the hardness level (~395Hv) of the as-received sheet material remains stable with aging at temperatures up to 800°C for the aging times tested. Isothermal aging at higher temperatures softens the materials rapidly initially, then more gradually with the hardness stabilizing at a constant level for each aging temperature. The lowest hardness value (~323Hv) was obtained upon aging at 1000°C after 144h. On the other hand, annealing at 1200°C rapidly reduced the hardness to a similar level, but annealing at still higher temperatures resulted in increasingly higher hardness.

3.3 Aging Responses

Figure 7 shows the strength variation against time for aging treatments conducted at temperatures between 700°C and 1000°C. The Vickers hardness (Hv) vs. time plots were made using the data from Figure 6. The scale showing the corresponding yield-strength (YS) values *(in MPa)* was *estimated* using the empirically determined relationships between Vickers hardness (Hv), Rockwell C hardness (RcH) and tensile yield strength (YS) as shown in Figure 8.

In this process, the relationship between RcH and YS values in the current sheet material was assumed to follow the consistent trend fit to the data in Figure 8a. That data was obtained from the measurements made on various gamma TiAl materials that include Ti-45.3Al-2.1Cr and experimental alloys [11], alloys K7 and K5 [12, 14] and PM wrought alloy 03K, having a range of composition of Ti-(44.8-47.4)Al-3Nb-0.2W-0.2B-0.2C-0.2Si) [13] and various microstructures. Within the range of measurements, the relationship is linear in a log-linear scale, as shown in Figure 8a, and can be expressed as

$$\text{Log (YS)} = 0.0217(\text{RcH}) + 2.06; \quad 25 < \text{RcH} < 45 \qquad (1)$$

Since the hardness values of the current sheet material were measured using the Vickers indentation method because of the thickness constraint, a supporting experiment was conducted to relate Vickers hardness (Hv) to RcH. In this experiment, 10mm thick samples were cut from an alloy 03G (Ti-45Al-1Cr-6Nb-0.2W-0.2B-0.4C-02Si) forging (that was available) and given various annealing and cooling treatments that would yield widely varying hardness values. Both Hv and RcH measurements were made on each sample and these were plotted in a linear space, as shown in Figure 8b. Within the range of the measured data, they are linearly proportional to each other and described by the following relationship

$$\text{RcH} = 0.110\ (\text{Hv}) - 4.20; \quad 300 < \text{Hv} < 450 \qquad (2)$$

By combining relation (1) and (B), YS and VH are related as

$$\text{Log(YS)} = 0.00239(\text{Hv}) + 1.969 \qquad (3)$$

Relation (3) was used to estimate the yield strength (YS) scale shown on the strength axis in Figures 6 & 7. The yield-strength level of the as-received sheet material is calculated to be 810MPa.

As the aging temperature increases, the strength level is lowered progressively faster with aging time and reaches a quasi-steady-state value that apparently is specific to each aging temperature (Figure 7). For example, a steady (or equilibrium state) strength level at 1000°C appears to be 323VH or 550MPa and is reached after 150h. The intrinsic strength at 900°C is expected be approximately 570MPa and that may be reached well after a 200h exposure. At 800°C, it will take 200h to reach a strength level of 760MPa, which is a relatively small strength reduction from the as-received condition. The measured strength decreases upon aging were reflected in the microstructures, and Figure 9 exemplifies such cases by comparing those microstructures that were obtained after aging at 900°C for 96h (Figure 9d) and 1000°C for 72h (Figure 9f). These may be compared to the as-received sheet microstructures (Figure 9b). In both aged conditions, especially at 1000°C, fine lamellar grains (present in Figure 9a and also described in Figure 3) transformed into featureless gamma-phase grains and twinned grains mostly disappeared. On the other hand, alpha-2-phase particles (imaged bright) became coarser and appear to have a role in pinning gamma-phase grains. This resulted in reducing the volume fraction of fine gamma-phase grains. After 1000°C/72h aging (Figure 9f), alpha-2-phase particles are further dispersed and fine gamma-phase grains became much fewer in number.

The alpha-2-phase coarsening process described above, that is increases to the average gamma-phase grain size, is manifested by the corresponding EBSD micrographs for the three different aging conditions shown in Figures 9a, c, and e, respectively. With aging, the average grain sizes as well as the number of grains having high-angle grain boundaries are increased, as listed in Table 2.

3.4 Annealing Response

Annealing at 1200°C and higher temperatures increases the hardness (Figure 6). This is reflected by the microstructure changes shown in Figure 10, where microstructure evolution upon high-temperature annealing (Figure 10b, c and d) is compared to that at 1000°C (Figure 10a). The alpha-2-phase (imaged bright) developed in the form of laths within lamellar grains whose volume increased as the annealing temperature was raised. This effectively enhances the strength level from 530MPa upon annealing at 1200°C, gradually to 560MPa after annealing at 1300°C and, more drastically to 810MPa upon annealing at 1350°C, as shown in Figures 6 and 10. Annealing at 1300°C (18°C below the alpha transus) resulted in a typical nearly-lamellar (NL)

microstructure, while annealing at 1350°C yielded a fully-lamellar microstructure having an average grain size of 71μm, Figure 1.

4. Discussion

4.1 Sheet Microstructures and Aging Response

The as received sheet microstructure consisted of a mixture of relatively coarse grains and fine grains that can be called a bimodal microstructure (Figure 3). The coarse grained microconstituent consisted of gamma-phase grains containing twins (Figure 3) together with featureless grains (Figure 3) that are imaged as lamellar grains having ultrafine lath structures (Figure 4b). The fine grained microconstituent consisted of gamma-phase grains whose grain boundaries are often pinned by alpha-2-phase having various shapes (Figure 4). The compositions of the coarse gamma-phase grains and lamellar grains are very different, as shown in Figure 11a. Their average compositions are as follows:

Coarse gamma-phase grains:	Ti-47.41Al-5.25Nb (in at%)	(4)
Lamellar grains:	Ti-42.9Al-5.36Nb (in at%)	(5)

The differences in Ti and Al content are likely to be the major reason why the overall composition in the as-received sheet material shows large variations (Figure 5). On the contrary, the Nb content is fairly constant (Figure 5), which is manifested by the fact that the contents of Nb are almost the same in both the gamma and alpha-2 phases.

As aging progresses, coarsening processes are taking place, Figure 9. During these processes, lamellar grains are transformed to gamma-phase grains forming coarse alpha-2-phase particles (see the alpha-2-phase particles in Figure 9b and c). Twinned grains disappear yielding featureless gamma-phase grains. In the fine gamma/alpha-2-phase mixture microconstituent, alpha-2-phase particles coarsen permitting the fine gamma-phase grains to grow. The resulting microstructures are a mixture of coarsened gamma-phase grains and coarsened alpha-2-phase particles (Figure 9f). Globally, this microstructure evolution process is highlighted by the EBSD micrographs (Figures 9a, c, *e*) where it is clearly shown that grain growth occurs largely at the expense of fine low-angle boundary grains (Table 2), thereby by narrowing the grain-size distribution.

At 1000°C, the steady-state condition appears to be reached after 144h (Figure 7), resulting in a microstructure that is similar to that of Figure 9f. The composition of gamma-phase grains was analyzed on 14 randomly selected grains using the EPMA, and the results are plotted in Figure 11b. Though not shown here, the coarse alpha-2-phase particles were also analyzed. Their compositions were found on average to be:

Gamma-phase grains:	Ti-46.22Al-5.24Nb (at%)	(6)
Alpha-2-phase particles:	Ti-35.61Al-5.31Nb (at%)	(7)

The compositions are considered to be those of the gamma phase and alpha-2 phase in equilibrium at 1000°C. Apparently, the entire Nb addition (5.43 at%, Figure 5) was accommodated, and the solubilities of Nb appear to be the same in both phases.

4.2 Strengthening Mechanisms

Over the last fifteen years several varieties of engineering gamma-TiAl alloys evolved toward improved temperature capability. With these advances, the Al content has been reduced while the Nb content increased and, the entire alloy family can be accordingly grouped as follows:

I Ti-48Al-2Nb based
II Ti-(46-47)Al-(2-3)Nb based
III Ti-45Al-(5-10)Nb based
IV Ti-45Al-(5-7)Nb-RM (refractory metals)

Observations suggest the strength levels were enhanced along with this composition-base evolution. The strength increases observed for the thermomechanically processed versions of the group III alloys, over those for groups I and II, were explained by the solid-solution hardening of the gamma phase; reportedly by having some of the Nb atoms take the Al sites instead of Ti sites [9]. This interpretation was recently questioned on the basis of an observed small difference (~0.2%) between the Ti and Nb contents in the phases of these alloys relative to the binary base alloys. Instead, structural refinement, such as the observed abundant twinning activity, was proposed to be responsible for the strengthening [10].

However, these explanations are incomplete in that they only consider part of either the intrinsic or extrinsic aspects of strength and, have neglected fundamental aspects such as deformation structures, changes in phase-boundary positions, phase volume fractions, microstructure evolution, and possible oxygen-solubility effects. There has been no effort to quantify the mechanisms or to perform mechanistic analysis. The strengthening mechanisms, especially in sheet material, appear to be complex and to explain them all of these aspects need to be considered.

On the basis of the observations described earlier, the overall strengthening behavior is shown in Figure 12. The yield strength (YS) of as-received sheet was estimated to be 810MPa and that was reduced to 550MPa after a full aging at 1000°C for 72h. At the same time, the average grain size was increased from 5.99 μm to 9.64 μm. According to the hardness curve (Figure 12a), these values are considered to be at the steady state. The steady-state microstructure (Figure 12c) consists of gamma-phase grains

free of twins and alpha-2-phase particles. The residual strength of 550MPa apparently results from the gamma- and alpha-2-phases by some rule of mixtures. Here we make estimates for three aggregated and additive contributions to the strength based on the microconstituents formed and their changes upon aging:

$$\sigma_t \text{ (Total)} = \sigma(\text{MS}) + \sigma(\text{HP}) + \sigma(\alpha_2) \qquad (8)$$

where σ_t is the initial sheet strength, σ(MS) is a microconstituent strengthening from unstable aspects (all events recovered during annealing) of the bimodal structure, σ (HP) is the gamma-phase boundary strengthening and $\sigma(\alpha_2)$ is a contribution from alpha-2-phase particles; the latter two being assumed stable before and after annealing. Thus, σ(MS) is assigned to the strength loss and, by difference is estimated at 260MPa. This consists of the changes to fine duplex-constituent strengthening, lamellar structure strengthening, twin strengthening and rolling texture strengthening that recover during annealing. The remaining strength of 550MPa includes the boundary strengthening, intrinsic strength and alpha-2-phase strengthening. These strengths then can be estimated as follows:

$$\sigma_t \text{ (Total)} = 810\text{MPa} \qquad (9A)$$

$$\sigma(\text{MS}) = 260\text{MPa} \quad \text{(Unstable microconstituent)} \qquad (9B)$$

$$f\sigma(\alpha_2) + (1\text{-}f)\sigma(\text{HP}) = 550\text{MPa} \quad \text{(Stabilized microconstituent)} \qquad (9C)$$

To obtain the values reflected in (9C), consider the following. The volume fraction of alpha-2 phase, f, is estimated to be about 5% from Figures 9f and 12c. The strength of alpha-2 phase is estimated to be roughly three times of that of gamma phase [15, 16]. This leads to (9C) being written as

$$0.05[3\sigma(\text{HP})] + 0.95\sigma(\text{HP}) = 550\text{MPa} \qquad (10A)$$

where σ(HP) is obtained from the intrinsic and grain-size strengthening of the gamma phase from prior studies [17]. Since from (9A) σ(HP) is 95% of the remaining strength of 550 MPa, reflecting this in a “Hall-Petch” strengthening relationship gives

$$\sigma(\gamma) = \sigma(\text{HP}) = \sigma_o + kd^{-1/2} = 500\text{MPa} \qquad (10B)$$

and by (9A) again, one must write

$$\sigma(\alpha_2) = 1{,}000\text{MPa} \qquad (10C)$$

Since k~1MPa√m for gamma-phase-grained microstructures [4, 5, 6] and here d=9.64μm (Table 2), the intrinsic strength is calculated to be σ_o = 178MPa. However, this intrinsic strength can be viewed as consisting of two components as follows:

$$\sigma_o = 178\text{MPa} = \sigma_o\,(\text{TiAl}) + \sigma_o\,(\text{Nb effect}) \qquad (11)$$

From prior work in the literature, the intrinsic strength for the TiAl gamma phase is approximated to be σ_o (TiAl) 80MPa from PST crystals [18] and the measurements of fine-grained ternary gamma material [19, 20]. Thus, the strength contribution by the addition of 5.4at% Nb is estimated to be about 100MPa. These are summarized below.

$$\sigma_o\,(\text{TiAl}) \sim 80\text{MPa} \qquad (12A)$$
$$\sigma_o\,(\text{Nb addition effect}) \sim 100\text{MPa} \qquad (12B)$$

This intrinsic strength increase of 100MPa by the addition of Nb is significant and, it is important to understand how and why it happens and to investigate if any other effects exist. This is discussed in the following sections.

4.3 Nb Effect on Intrinsic Strength

The addition of Nb will alter the positions of the phase boundaries, which will change not only the partitioning of alloying elements but also the volume ratio of constituent phases.

An isothermal section (1000°C) of the ternary Ti-Al-Nb phase diagram was constructed around the current sheet alloy composition, **T** (Ti-44.7Al-5.3Nb, Figure 5) and the binary composition **B** (Ti-44.7Al), as shown in Figure 13. In figure 13, the construction was based on the measured equilibrium compositions (**C3** and **C4)** of gamma and alpha-2 phases (from Figure 11b and relations f and g) and the phase-boundary positions (**C1** and **C2**) taken from the equilibrium binary Ti-Al phase diagram [21]. All of these compositions are listed below.

T: Ti-44.7Al-5.4Nb	(Current ternary sheet alloy)
C3: Ti-45.7Al-5.3Nb	(Gamma-phase in alloy **T**)
C4: Ti-35.6Al-5.2Nb	(Alpha-2-phase in alloy **T**)
B: Ti-44.7Al	(Base binary alloy)
C1: Ti-48.5Al	(Gamma-phase in alloy **B**)
C2: Ti-36.5Al	(Alpha-2-phase in alloy **B**)

Figure 13 shows that adding Nb into the binary system shifts both ($\gamma/\gamma+\alpha_2$) and $\alpha_2/\alpha_2+\gamma$) phase boundaries to the Ti-rich side, with the former moving substantially and the latter shifting only slightly.

These result in changes to the composition as well as volume fraction of constituent phases. In the current sheet alloy **T**, which was produced by adding 5.4at%Nb into the binary base alloy **B** (Ti-44.7Al), the Nb addition reduced the Al content in the gamma phase by 2.8at% (**C1** to **C3**). Since the added Nb is likely to take Ti sites [22-24], the vacated Al sites (2.8 at%) will be filled by Ti, thereby yielding solution hardening of the gamma phase. This is not a simple replacement as has been assumed by other reporters [9] since the Nb has a strong site preference within the $L1_0$ structure. Rather, the Nb addition results in an increase of solute content (Ti atoms expelled by Nb) on the Al sites, and this is considered to be the main source of the enhanced intrinsic strength of 100MPa (see relation 10B). Solution hardening by an addition of Nb was also reported for PST crystals in that a PST crystal of Ti-49Al-1.2Nb showed a higher yield strength by 35MPa in the easy orientation over a Ti-49Al PST crystal [18].

While the gamma phase is solution strengthened by the Nb addition, the ternary alloy system loses some strength overall through a drastic reduction (by 75%) of alpha-2 phase volume fraction (**T-C3** vs. **B-C1** in Figure 13). Since the strength contribution to the alloy **T** by the 5vol% alpha-2-phase contribution is ~50MPa (relation 10C), the contribution of alpha-2-phase to the strength in the binary alloy **B** is estimated to be 200MPa. The loss of ~150MPa by the reduction of alpha-2-phase volume fraction is more than the gain by the solid-solution hardening from the Nb addition in the alloy **T.** This is consistent with the report that Ti-45Al showed slightly greater strength than the Ti-45Al-5Nb for fully-lamellar conditions [25]. When alloy **T** (Ti-45Al-5Nb) is measured to be stronger than alloy **B** (Ti-45Al) in fully-aged conditions, that is most likely due to the finer grain sizes usually attained by the Nb addition. When both alloys are tested in processed and only partially-aged conditions, the ternary alloy will obtain additional strengthening due to twinning of gamma-phase grains [Figure 3], which has been reported to occur more abundantly in Nb-containing alloys [10].

4.4 Oxygen Effect on Intrinsic Strength

There is a possibility that oxygen contributes to the increased intrinsic strength of Nb-containing alloys. It has been known that the oxygen solubility in the gamma phase (Ti~48 base) is roughly 300ppm (atomic) at temperatures below 1100°C [26]. A recent prediction, based on the oxygen atoms taking Ti6 octahedral cavities [27], has shown that the solubility is a strong function of Al content in the gamma phase [28]. These predicted data are plotted against the Al contents in the constituent phases (**C3** for gamma and **C4** for alpha-2 in Figure 13) for the present alloy **T,** as shown in Figure 14. It is estimated that the oxygen solubility is about 4 at% and greater than 2000 atppm in the respective constituent alpha-2 and gamma phases. Since the oxygen content in alloy **T** is assumed to be between 2000 and 2600 at-ppm (800-1000 wt-ppm) and the volume fraction of alpha-2 phase is about 5%, the oxygen can be partitioned to the gamma-phase TiAl in an amount up to ~600 at-ppm, which is twice of the maximum

solubility in the binary alloy B (Ti-45Al). If that happens, it is expected to strengthen the material by solution hardening.

5. Summary & Conclusions

As-produced Gamma Met PX sheet material, having a nominal composition of Ti-45Al-5Nb, exhibits a characteristic complex, bimodal microstructure that consists of twinned gamma-phase grains, fine-lath lamellar grains, and regions of very fine gamma-phase grains pinned by alpha-2-phase particles.

This structure is thermally unstable above 840°C and, aging at 900°C or 1000°C equilibrates the phases and the structure, eventually yielding a simple, stabilized microstructure that consists of a coarsened gamma-phase-grain matrix dispersed with coarsened alpha-2-phase particles.

The alloy in the as-produced sheet form is strengthened by the contributions from the unstable structures, grain-boundary strengthening, and solution strengthening of the gamma phase.

The solution strengthening is derived as a result of the Nb addition which shifts the gamma-phase boundary to the Ti-rich side of the phase diagram, thereby increasing the number of Al sites available for Ti atoms expelled by incoming Nb. The decreased Al content in the gamma phase increases the available interstitial octahedral Ti sites for oxygen, leading to a possibility of further solution hardening of the matrix by oxygen.

While the Nb addition results in strengthening of the alloyed material by increasing the intrinsic strength, it significantly reduces the volume fraction of the alpha-2 phase that is roughly three times stronger than the gamma phase. This loss is greater than the gain by solid-solution hardening. This explains why the measured strengths are similar between Ti-45Al-5Nb and Ti-45Al in thermo-mechanically processed conditions, in spite of the possibly of a greater contribution by twin strengthening in the ternary alloy.

Acknowledgments: S-L. Kim is acknowledged for her dedicated microscopy and analysis. We thank Drs. P. Martin and L. Semiatin for their technical discussions. The work was performed at Air Force Research Laboratory under AF Contract No. F33615-01-C-5214.

References

1. S.L. Semiatin, S.M. El Soudani, D.C. Vollmer and C.R. Thompson, US Patent, No. 5,442,847, August 22, 1995.

2. H. Clemens, et al., in *Gamma Titanium Aluminides,* eds. Y-W. Kim, D. Dimiduk and M. Loretto, TMS, Warrendale, PA, USA (1999) 209-223.

3. H. Kestler, N. Eberhardt and S. Knippscheer, in *Niobium High Temperature Applications*, eds. Y-W. Kim and T. Carneiro, TMS, Warrendale, PA (1997) 167-181.

4. F. Appel, M. Oehring and R. Wagner, Intermetallics 8 (2000) 1283-1321.

5. Y-W. Kim, in Niobium High Temperature Applications, eds. Y-W. Kim and T. Carneiro, TMS, Warrendale, PA (2004) 125-137.

6. G.L. Chen, W.J. Zhang, Z.C. Liu, S.J. Li, and Y-W. Kim, in *Gamma Titanium Aluminides,* eds. Y-W. Kim, D.M. Dimiduk and M.H. Loretto, TMS, Warrendale, PA (1999) 371-380.

7. T. Tetsui, in *Niobium High Temperature Applications*, eds. Y-W. Kim and T. Carneiro, TMS, Warrendale, PA (1997), 205-213.

8. T. Tetsui and S. Ono, Intermetallics, 7 (1999) 689-697.

9. W.J. Zhang, S.C. Deevi, and G.L. Chen, Intermetallics, 10 (2002) 403-406.

10. F. Appel, M. Oehring, J.D.H. Paul, and U. Lorenz, in *Structural Intermetallics 2001*, eds. K.J. Hemker, D.M. Dimiduk, H. Clemens, R. Darolia, H. Inui, J.M. Larsen, V.K. Sikka, M. Thomas, J.D. Whittenberger, TMS, Warrendale, PA (2001) 63-72.

11. D.M. Dimiduk, P.M. Hazzledine, T.A. Parthasarathy, S. Seshagiri, and M.G. Mendiratta, Met Trans A, Vol. 29A (1998) 37-47.

12. Y-W. Kim, Unpublished test results (2001).

13. S. Russ, C. Woodward, Y-W. Kim, and F. Yolton, in *Structural Aluminides for High Temperatures*, eds. Y-W. Kim, D. Morris, C. Leyens and R. Yang, TMS, Warrendale, PA (2008) 51-60.

14. Y-W. Kim, Mater. Sci. & Eng., A192/193 (1995) 519-533.

15. T. Nakano and Y. Umakoshi, J. of Alloys and Compounds, 197 (1993) 17-20.

16. H. Inui, Y. Toda and M. Yamaguchi, Phil. Mag. A, 67 (No. 6) (1993) 1315-32.

17. Y-W. Kim, Intermetallics 6 (1998) 623-628.

18. T. Nakano, A. Yokoyama and Y. Umakoshi, Scripta Met. Mater. 27 (1992) 1253-1258.

19. S.C. Huang and D.S. Shih, in Microstructure/Property Relationships in Titanium Aluminides and Alloys, ed. Y-W. Kim and R.R. Boyer, TMS, Warrendale, PA (1990) 105-122.

20. C. Koeppe, A. Bartels, J. Seeger and H. Mecking, Metall. Trans. A, 24A (1993) 1795-1806.

21. Y-W. Kim, Acta Metal. Mater., 40, No. 6 (1992) 1121-1134.

22. C. Woodward, S. I. Rao and D.M. Dimiduk, JOM (1998) 37-42.

23. D. M. Dimiduk, Intermetallics, 6 (1998) 613-621.

24. R. Yang, Y. Hao, Y. Song and Z-X. Guo, Z. Metallkd, 91 (2000) 296-301.

25. J.D.H. Paul, F. Appel and R. Wagner, Acta Mater., 46 (No. 4) (1998) 1075-1085).

26. S. Gerstl, Y-W. Kim and D. Seidman, Interface Science 12 (2004) 303-310.

27. A. Menand, A. Huguet and A. Nerac-Partaix, Acta Mater., 44 (1996) 4729.

28. W. Lefebre, A. Loiseau and A. Menand, in *Gamma Titanium Aluminides*, eds. Y-W. Kim, H. Clemens and A.H. Rosenberger, TMS, Warrendale, PA (2003) 63-74.

Figure Captions

Figure 1: BSEI of the microstructure on the rolling plane (L) of the as received sheet (PX0-L): Other planes, ST (short transverse) and LT (long transverse), are defined with respect to the rolling direction (RD).

Figure 2: PX0; Mid section of thickness planes of as received sheet

Figure 3: The microstructure taken from a TEM foil made of the as received sheet (PX0-L). The micrograph was made using the EBSD imaging system.

Figure 4: BSEI of PX0 (L) Microstructure taken from the same TEM foil used for Figure 3 micrograph. Figure 4a shows an overall view of the complex microstructure (see text) and Figure 4b shows a magnified view of the insert area in (a), revealing coarse, twinned gamma grains (G), coarse alpha-2 grains where lamella formation is incomplete (L), and area of fine gamma grains pinned by alpha-2 particles (F)

Figure 5: Compositional distribution determined by electron probe micro analysis along a length of 3200µm on two planes, ST (a, c) and L (b, d), of as-received sheet specimens

Figure 6: Vickers hardness values measured at RT plotted as a function of heat treatment conditions. Corresponding yield-strength values estimated from the relations depicted in Figure 8 are written on the Y-axis.

Figure 7: The effect of isothermal aging at different temperatures on Vickers hardness variation plotted using the data from Figure 6. YS estimated from Figure 8.

Figure 8: (a) Relationship between Rockwell hardness values and yield strengths previously measured on bulk samples of various gamma alloys (see text). The relationship shows a log-linear fit and (b) Vickers and Rockwell hardness values measured on bulk specimens of a gamma alloy in various annealing conditions showing a linear relationship.

Figure 9: Effect of aging on ST microstructures showing the progress of recrystallization from as-received (a, b) to 900°C/96h (c, d) and 1000°C/72h (e, f). Also shown via EBSD are the micrograph respective average GS and YS (a, c, e) and the distribution/morphology (bright α_2 and gray γ) shown in BSEI (b, d, f). (a) GS = 5.99µm and YS=840MPa, (c) GS = 6.75µm and YS ~585MPa and (e) GS = 9.64µm and YS ~ 480MPa.

Figure 10: Microstructure evolution upon high temperature annealing showing corresponding grain sizes (GS) and yield strengths (YS).

Figure 11: Compositional variation determined by EPMA in (a) coarse grains of as-received sheet samples (similar to those shown in Figure 9a) and, in (b) gamma grains after aging at 1000°C for 144h (similar to those in Figure 9b.

Figure 12: The evolution of hardness and estimated strength levels upon isothermal annealing, showing the YS at 1000°C (~550MPa) consisting of the HP strength and that of α_2 phase (a). The strength loss (260MPa) from the initial YS (~810MPa) is the effect of microstructure instability, σ(MS), which is apparent by comparing the initial microstructure with an average GS of 6.0µm (b) and the equilibrated microstructure with an average GS of 9.6µm (c).

Figure 13: Schematic isothermal (1000°C) phase diagram of the Ti-Al-Nb system showing a portion containing Ti-45Al (**B**) and Ti-45Al-5Nb (**T**) compositions. The phase fields were constructed based on the measured compositions of constituent phases in each alloy: **C1** and **C2** in alloy **B** from the available Ti-Al phase diagram [21]; **C3** and **C4** in alloy **T** that were measured (see Figure 11b and relations 6 and 7).

Figure 14: Solubility of oxygen in alpha, alpha-2 and gamma phases in binary Ti-Al alloys [28] plotted against the Al contents in the constituent phases in the current alloy T (Ti-44.7Al-5.3Nb).

Figures (14)

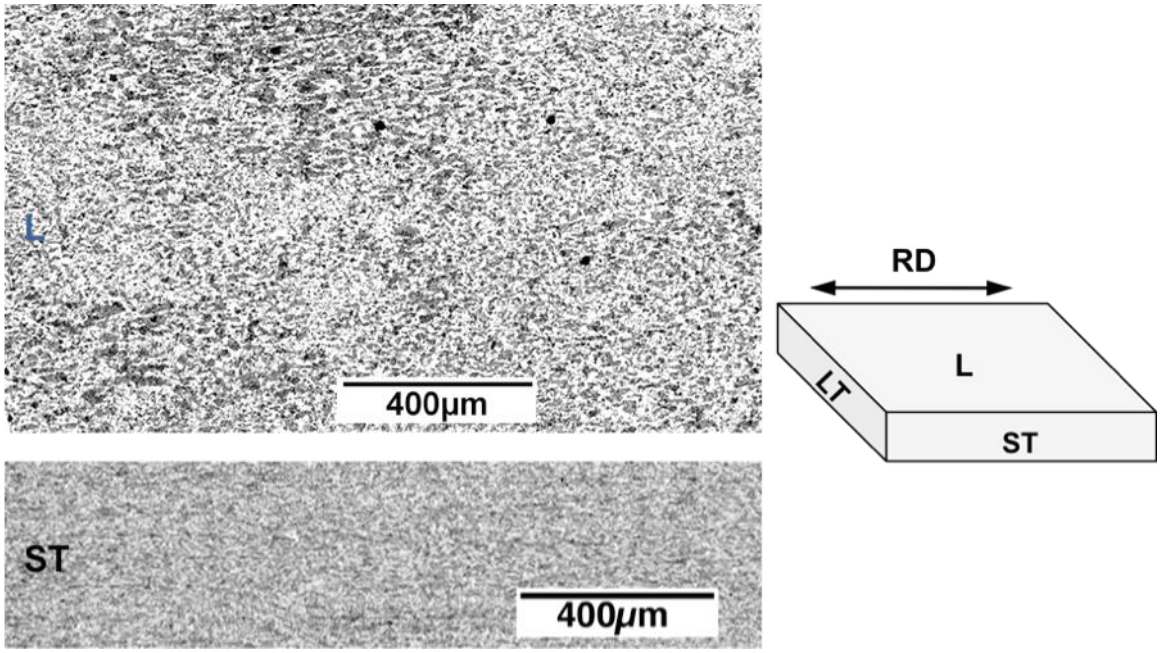

Figure 1

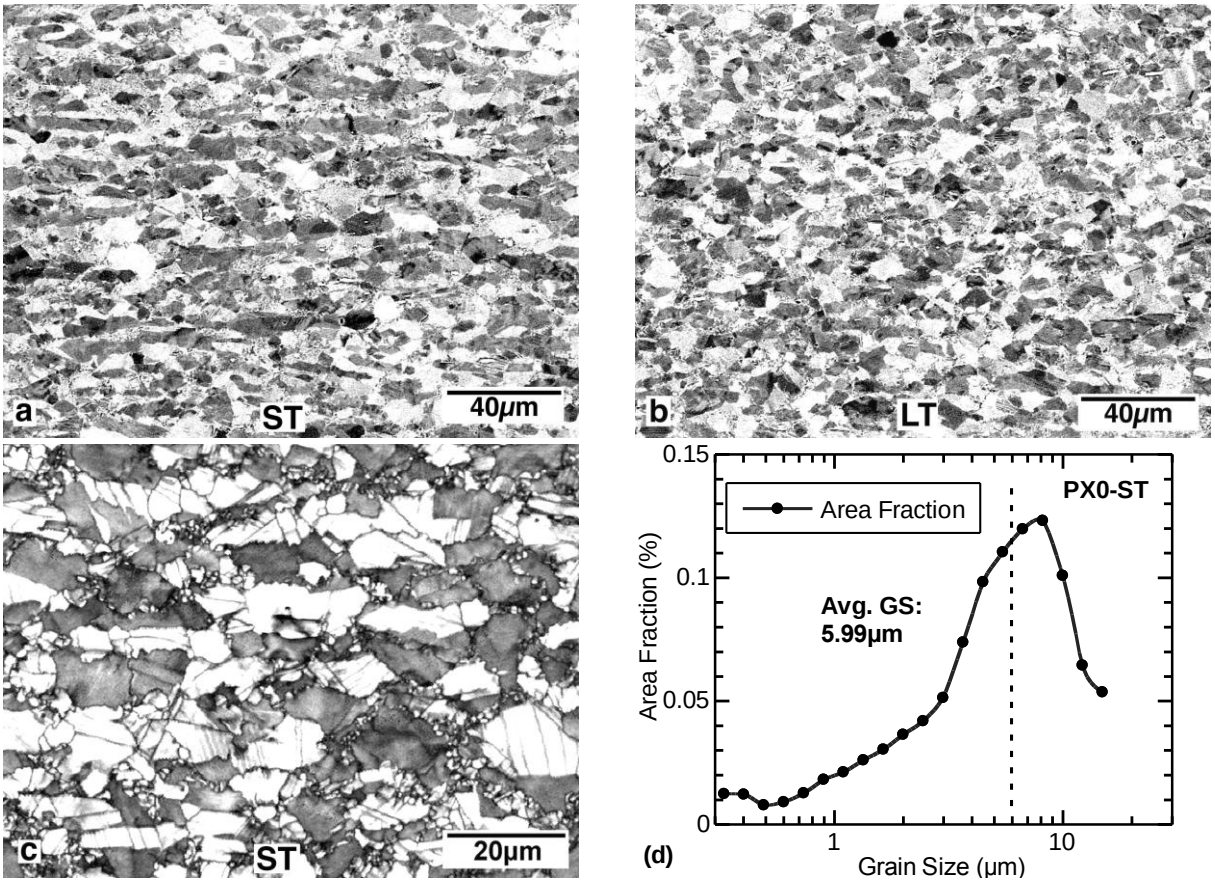
a
ST
40μm
b
LT
40μm
c
ST
20μm
(d)
PX0-ST
Area Fraction
Avg. GS:
5.99μm
Area Fraction (%)
0.15
0.1
0.05
0
1
10
Grain Size (μm)

Figure 2

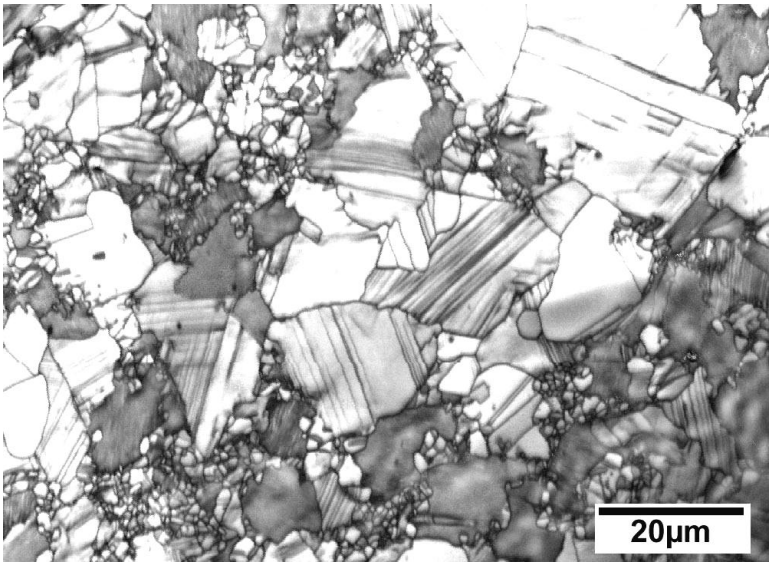

Figure 3

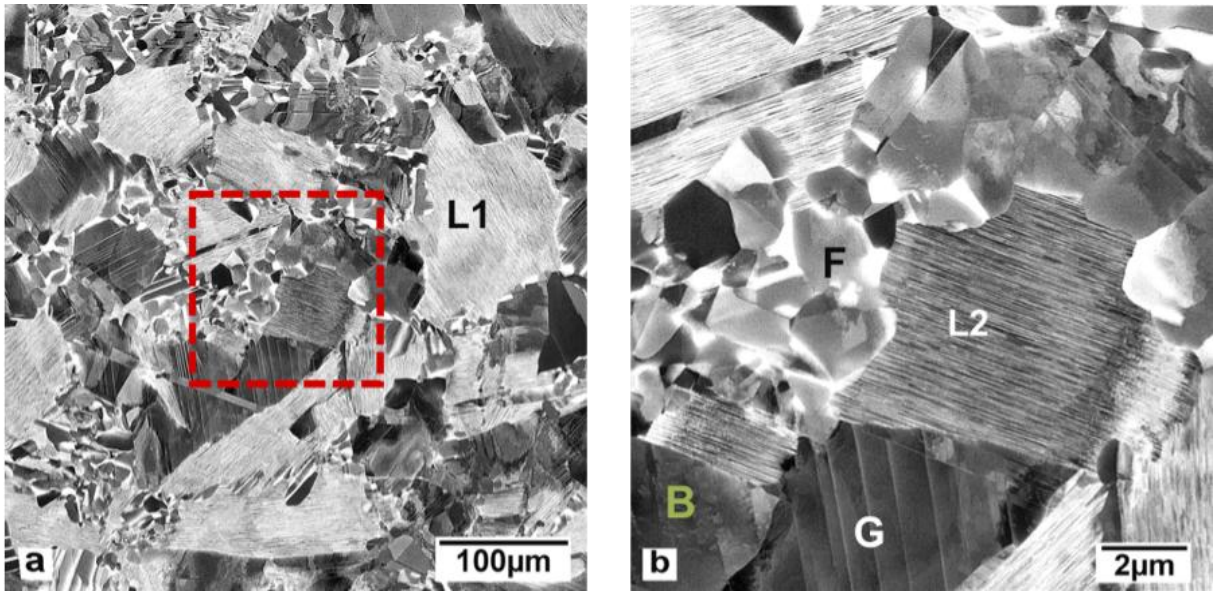

Figure 4

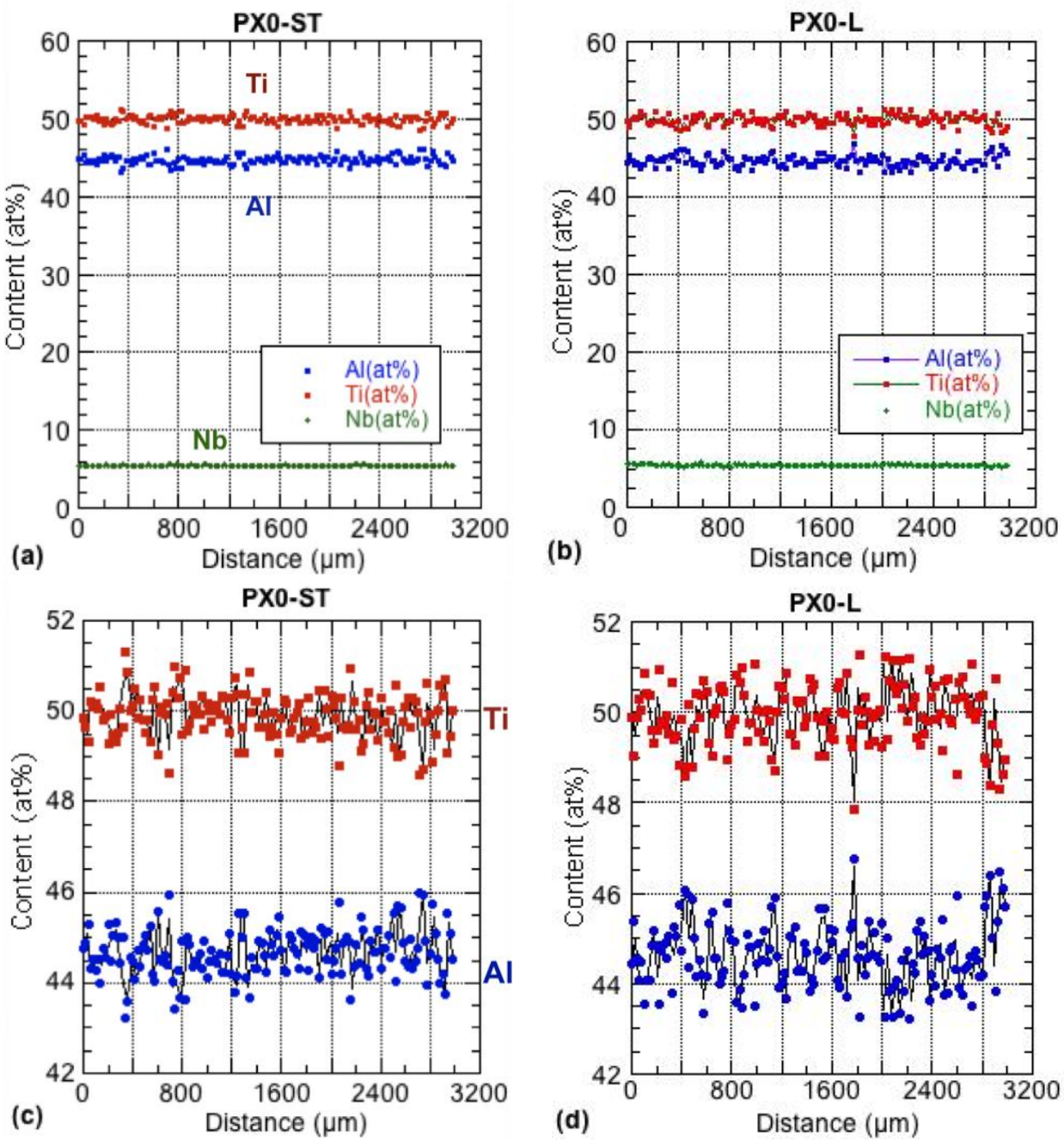

Ti-44.66Al-5.43Nb (ST)

Ti-44.63Al-5.43Nb (L)

Figure 5

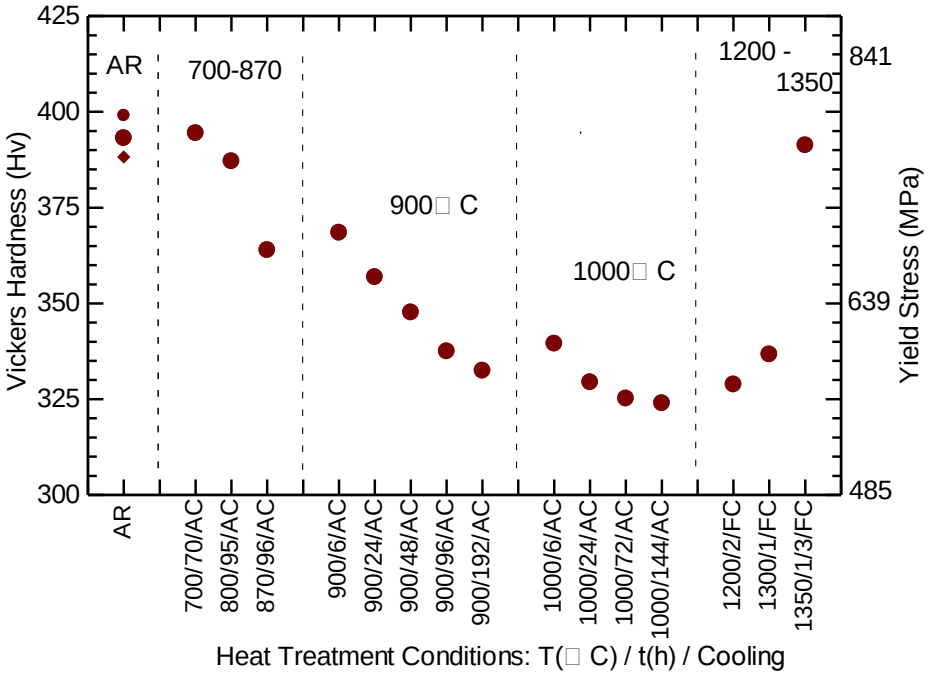

Figure 6

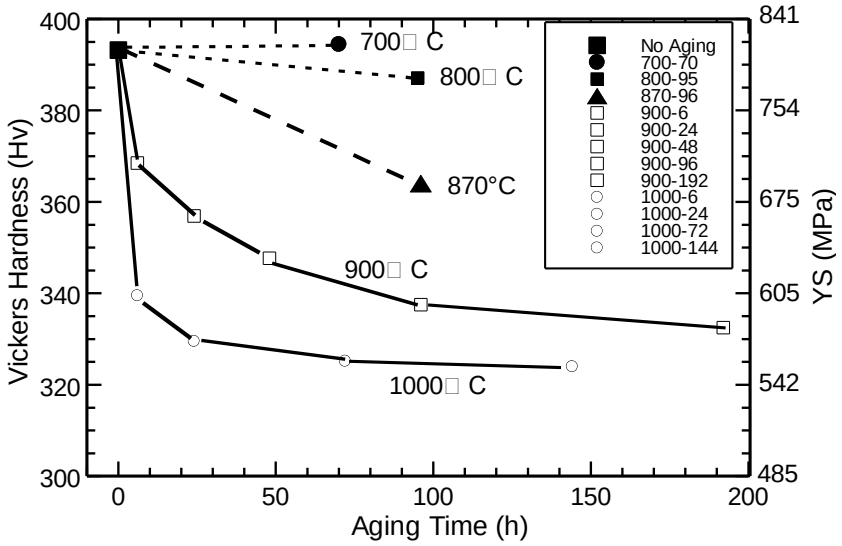

Figure 7

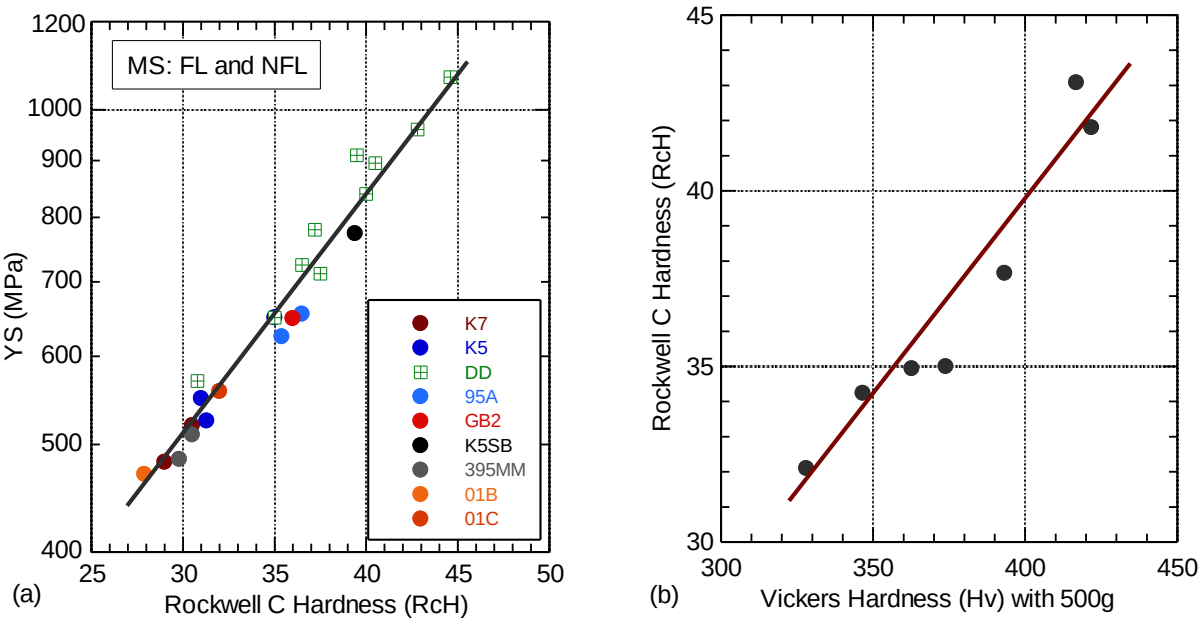
MS: FL and NFL
YS (MPa)
Rockwell C Hardness (RcH)
(a)
K7
K5
DD
95A
GB2
K5SB
395MM
01B
01C
Rockwell C Hardness (RcH)
Vickers Hardness (Hv) with 500g
(b)

Figure 8

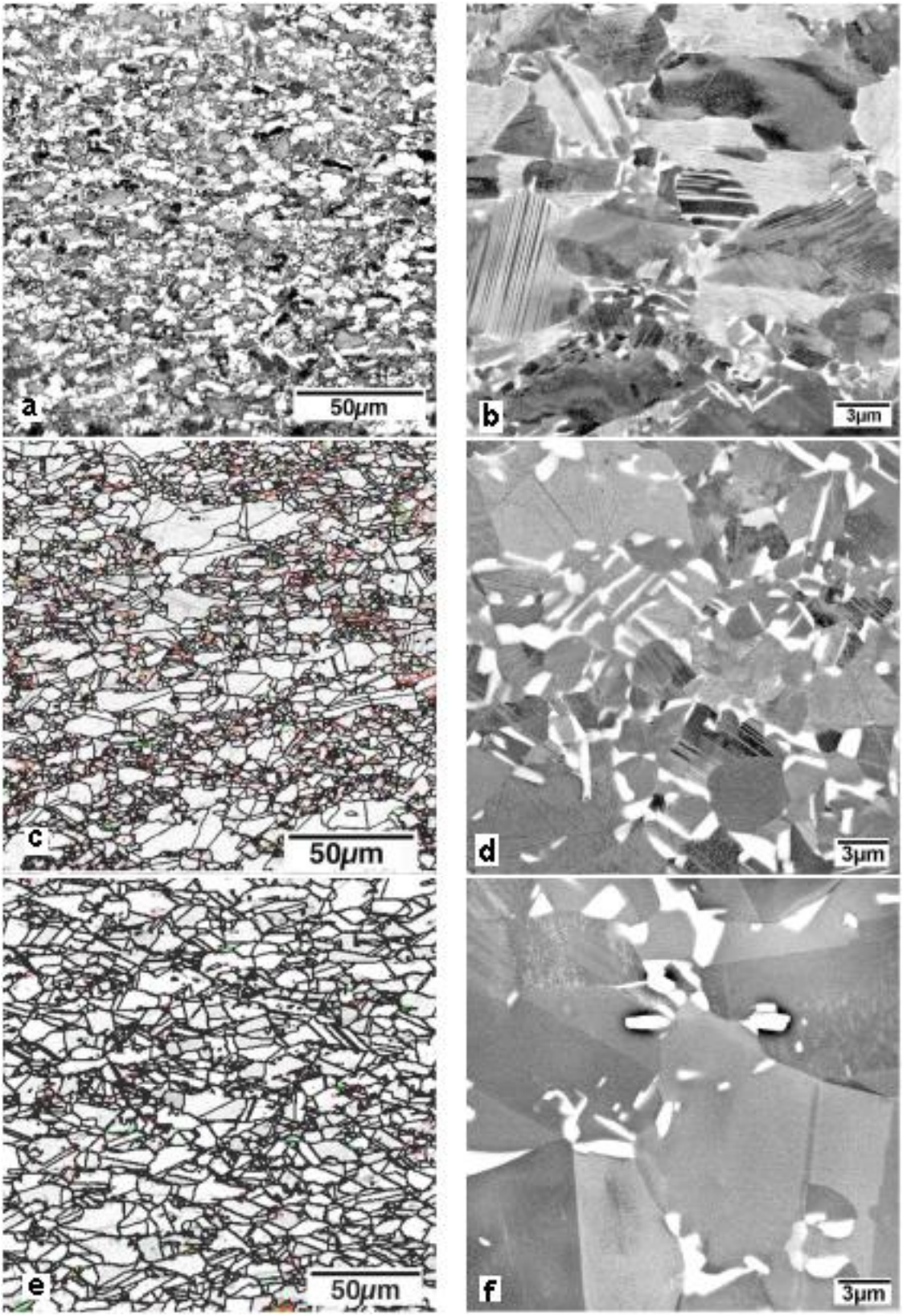

Figure 9

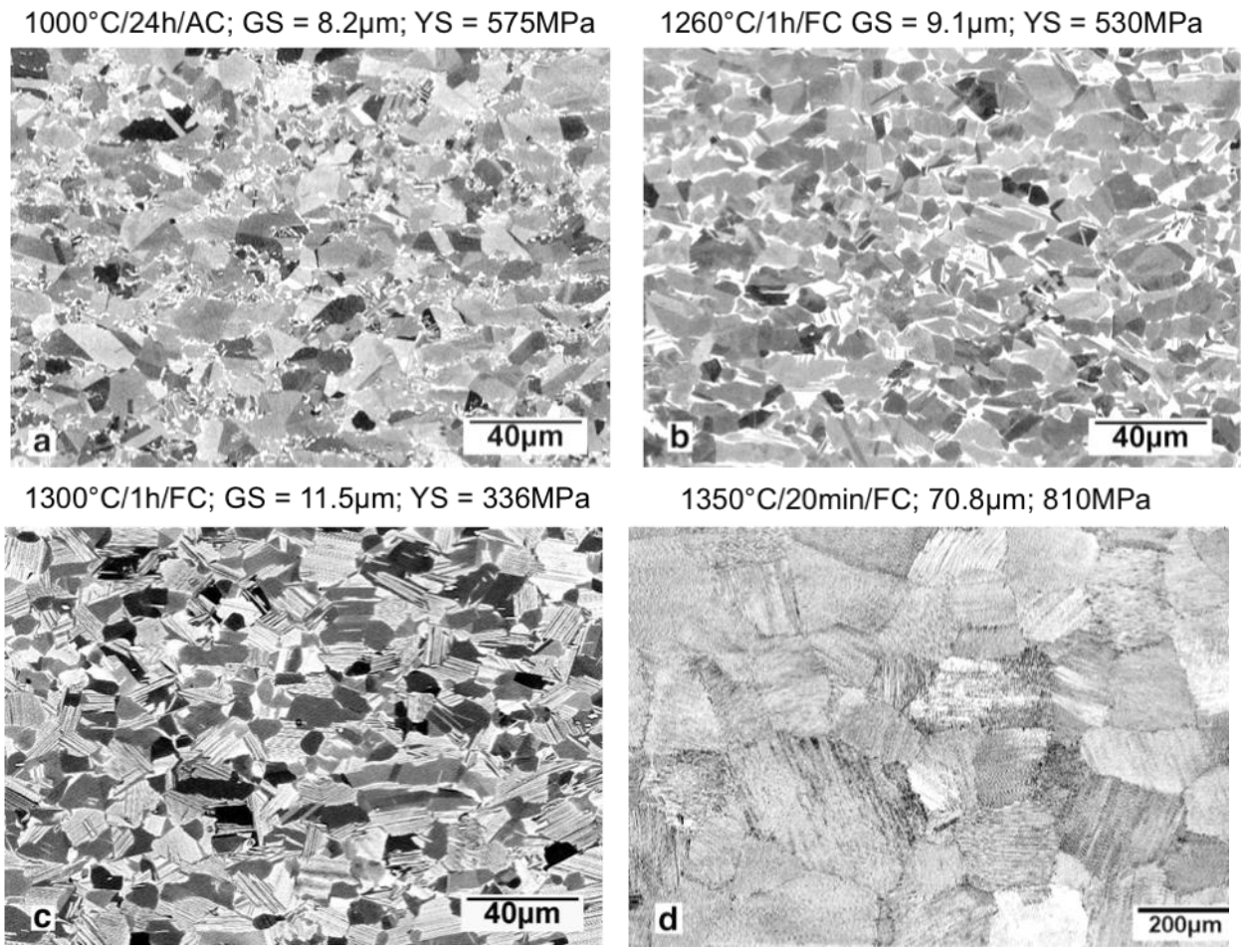
1000°C/24h/AC; GS = 8.2μm; YS = 575MPa
1260°C/1h/FC GS = 9.1μm; YS = 530MPa
a
40μm
b
40μm
1300°C/1h/FC; GS = 11.5μm; YS = 336MPa
1350°C/20min/FC; 70.8μm; 810MPa
c
40μm
d
200μm

Figure 10

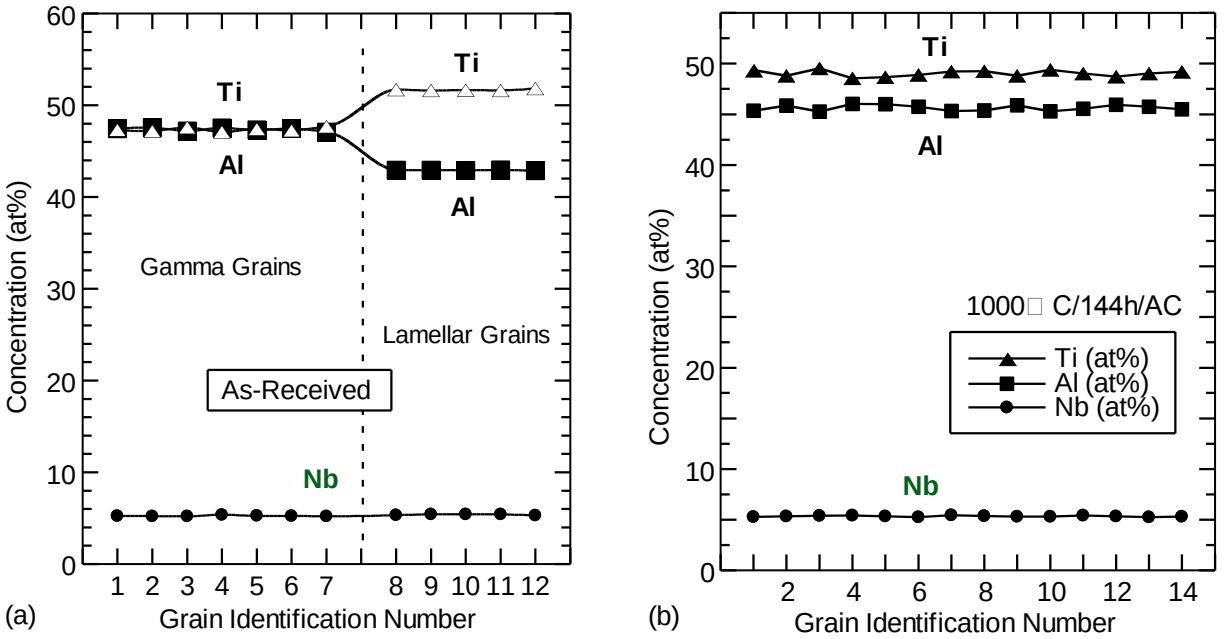

Gamma Grains: Ti-47.41Al-5.25Nb
Lamellar Grains: Ti-42.9Al-5.36Nb

Gamma Grains: Ti-45.68Al-5.34Nb
Alpha-2 Particles: Ti-35.61Al-5.21Nb

Figure 11

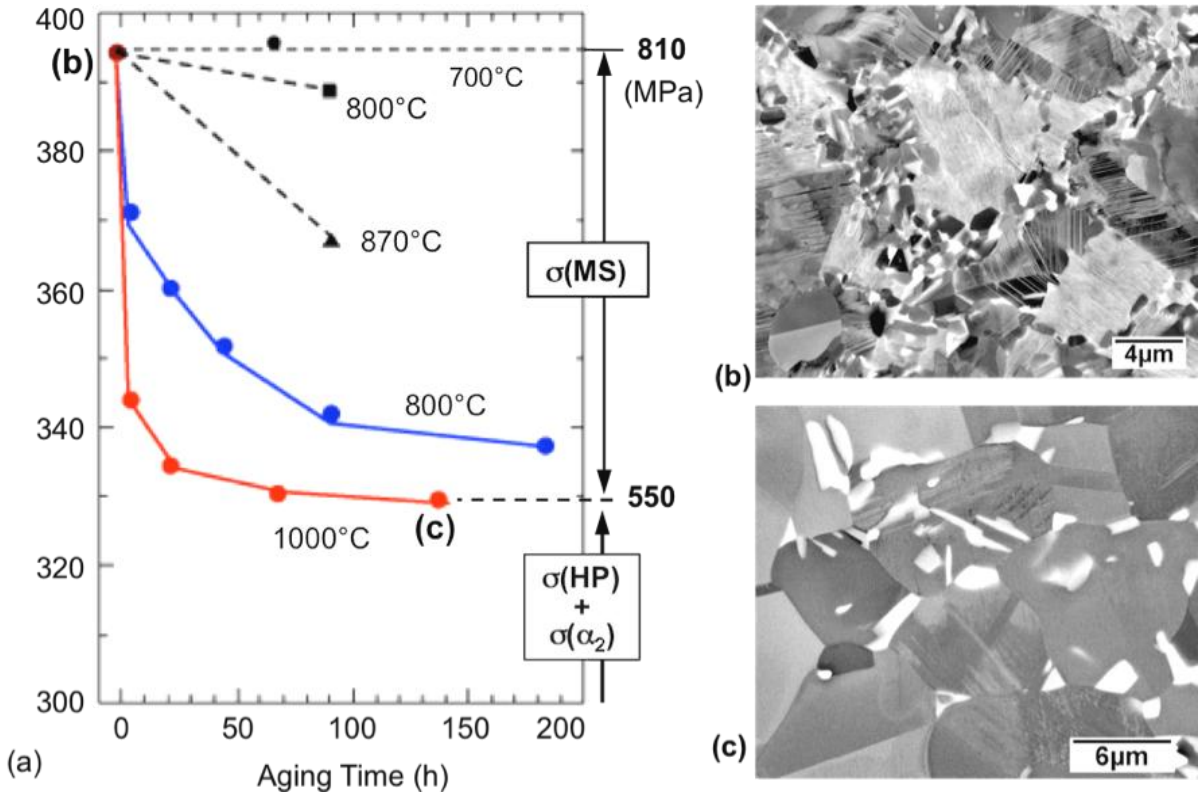

Figure 12

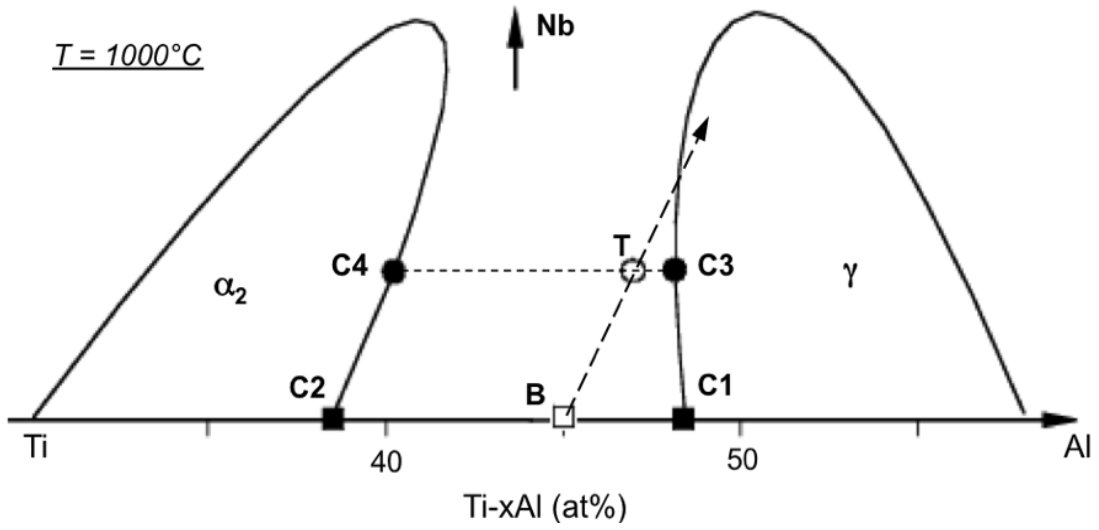

Figure 13

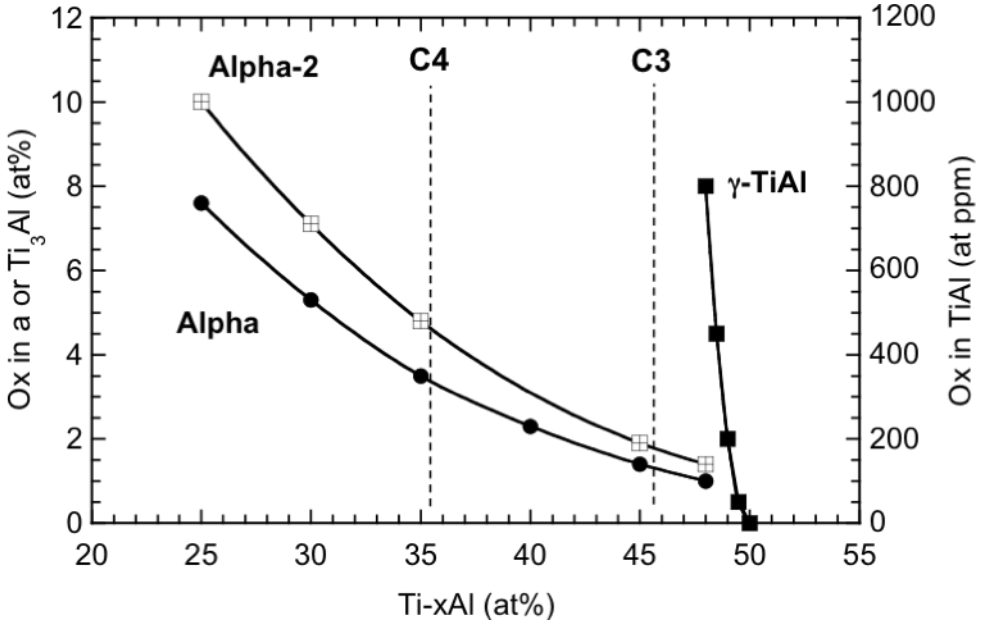
Alpha-2
C4
C3
γ-TiAl
Alpha
Ox in a or Ti3Al (at%)
Ox in TiAl (at ppm)
Ti-xAl (at%)
0
2
4
6
8
10
12
0
200
400
600
800
1000
1200
20
25
30
35
40
45
50
55

Figure 14

Tables (2)

Table 1: Heat Treatment Conditions and Characterized Planes

Group ID	HT Conditions	Env.	Observed Planes
PX0	Pack-Rolled + 1000°C/2h	Vacuum	ST, LT, L
PXA	(1200-1350)°C / (20m-1h) / FC	Vacuum	ST
PXB	1000°C / (6-144)h / AC	Ar	ST
PXC	900°C / (6-192)h / AC	Ar	ST
PXD	(700-870)°C / (70-96)h/AC	Ar	ST

FC: Furnace cooling; AC: Air-cooling; Env: Heat treatment environment; The faces used for observations and hardness measurements are ST (short transverse plane), LT (long transverse) and L (sheet face or rolled plane), as defined in Figure 1.

Table 2: Average Grain Size and High Angle Grain-Boundary Fraction vs. Aging

Aging Condition	Analyzed Area	Avg GS (μm)	HA GB Fraction (%)
As Received	Fig. 9a	5.99	87.6
900°C/96h	Fig. 9c	6.75	94.2
1000°C/72h	Fig. 9e	9.64	98.4

Avg (Average); GS (Grain size); HA GB (High-angle grain boundary)